FUNCTIONALIZATION AND CHARACTERIZATION OF SULFONATED POLY(STYRENE-ISOBUTYLENE-STYRENE) MEMBRANES FOR FUEL CELLS AND SPECIALTY SEPARATION APPLICATIONS

by

Sonia L. Avilés Barreto

Dissertation submitted in partial fulfillment of the requirements for the degree of

DOCTOR OF PHILOSOPHY
in
CHEMICAL ENGINEERING

UNIVERSITY OF PUERTO RICO
MAYAGÜEZ CAMPUS

2014

Approved by:

David Suleiman Rosado, PhD President, Graduate Committee	Date
María C. Curet-Arana, PhD Member, Graduate Committee	Date
Agnes Padovani, PhD Member, Graduate Committee	Date
L. Antonio Estévez De Vidts, PhD Member, Graduate Committee	Date
Sandra Coutin Rodicio, PhD Graduate Studies Representative	Date
Aldo Acevedo, PhD Chairperson of the Department	Date

ABSTRACT

In this study, the transport properties of poly(styrene-isobutylene-styrene) (SIBS) block copolymer were determined as a function of sulfonation level (0-94.9 %), counter ion substitution (Ba^{+2}, Ca^{+2}, Mg^{+2}, Mn^{+2}, Cu^{+2}, K^{+1}), single-walled carbon nanotubes (SWCNTs) functionalization (carboxylic groups, aminomethanesulfonic acid and p-aminobenzoic acid), SWCNT loading (0.01, 0.1 and 1.0 wt.%), and blends with radial poly(styrene-isoprene) for direct methanol fuel cell (DMFC) and chemical and biological protective clothing (CBPC) applications. Increasing the sulfonation level improved the ion exchange capacity (IEC) of the membranes up a maximum, suggesting a complex 3-D network at high sulfonation levels. Results show that proton conductivity increases with IEC and is quite sensitive to hydration levels and the type of water (i.e., bound or bulk) inside these proton exchange membranes (PEM). Methanol permeability, although also sensitive to IEC, shows a different behavior than proton conductivity suggesting fundamental differences in their transport mechanism. The incorporation of counter ion substitution decreases both methanol and proton transport. Methanol permeability seems to be related to the size of the studied counter ions, while proton conductivity is more sensitive to water content, which is also reduced upon the incorporation of counter ions. Methanol permeability is sensitive to SWCNTs addition, since its transport mechanism seems to be controlled by their presence and loading. The addition of radial poly(styrene-isoprene) creates unique morphologies that lead to high water uptake, poor interconnectivity of sulfonic groups and low methanol permeability. Selectivity (i.e., proton conductivity/methanol permeability) of the studied membranes was determined and compared to Nafion® 117 to complement the studies. Values suggest an optimum SWCNT loading (0.1 wt.%) for the highest sulfonation level studied with this functionalization (SIBS 89.7). Additionally, the SWCNT functionalization with sulfonic groups improves the transport properties of the sulfonated PEM. The efficiency of the membranes to separate dimethyl methylphosphonate (DMMP), the simulant of the chemical warfare agent Sarin, and water vapor also shows high values for the sulfonated and nanocomposite membranes. Vapor permeability studies suggest that the combination of ionic domains with unique morphological arrangements can lead to high separation efficiencies for CBPC application.

RESUMEN

En este estudio, se determinaron las propiedades de transporte del copolímero en bloques poli(estireno-isobutileno-estireno) (SIBS) en función de su nivel de sulfonación (desde 0 a 94.9 %); sustitución catiónica (Ba^{+2}, Ca^{+2}, Mg^{+2}, Mn^{+2}, Cu^{+2} , K^{+1}), tipo de funcionalización (grupos carboxílicos, ácido aminometansulfónico, y ácido para-aminobenzoico) realizada a nanotubos de carbono de pared única (SWCNT, por sus siglas en inglés); y concentración de dichos nanotubos (0.01, 0,1 y 1.0 % p/p); además de la adición de poli(estireno-isopreno) radial para celdas de combustible de metanol y ropa de protección contra agentes químicos y biológicos. El aumento en el nivel de sulfonación mejoró la capacidad de intercambio iónico de las membranas (IEC, por sus siglas en inglés) hasta un máximo, lo que sugiere la formación de una red tridimensional compleja a niveles altos de sulfonación. Los resultados muestran que la conductividad protónica aumenta con el IEC y es sensible a los niveles de hidratación y tipo de agua en la membrana (es decir, ligada o no ligada) dentro de estas membranas de intercambio protónico. La permeabilidad al metanol, aunque también sensible a la IEC, muestra un comportamiento diferente lo cual sugiere diferencias fundamentales en el mecanismo de transporte. La sustitución catiónica disminuye tanto el transporte de protones como el de metanol. La permeabilidad al metanol parece estar relacionada al tamaño del catión estudiado, mientras que la conductividad protónica es más sensible al contenido de agua, que también se reduce con la incorporación de cationes. La permeabilidad de metanol es sensible a los nanotubos de carbono ya que el mecanismo de transporte parece estar controlado por la presencia y concentración de los mismos. La adición de poli(estireno-isopreno) radial crea morfologías únicas que conducen a alta absorción de agua, pobre interconexión de grupos sulfónicos y baja permeabilidad al metanol. Para complementar los estudios, se determinó la selectividad de las membranas estudiadas (es decir, conductividad protónica/permeabilidad al metanol) y se comparó con Nafion® 117 . Los valores sugieren una carga óptima de nanotubos de carbono (0.1% en peso) para el nivel de sulfonación más alto estudiado con esta funcionalización (SIBS 89.7). Además indican que la funcionalización de nanotubos de carbono con grupos sulfónicos mejora las propiedades de transporte de la membrana de intercambio protónico. La eficiencia de las membranas para separar metilfosfonato de dimetilo (DMMP, por sus siglas en inglés)

utilizado como simulador del agente químico químico Sarín, y vapor de agua, también muestran valores altos para las membranas sulfonadas y nanocompuestas. Los estudios de permeabilidad de vapor sugieren que la combinación de dominios iónicos con arreglos morfológicos únicos puede conducir a altas eficiencias en la separación para aplicaciones de ropa protectora de protección de agentes biológicos y químicos.

To my parents
José Luis Avilés Rodríguez and
Sonia M. Barreto Soto, and my
sister Sully Mar Avilés Barreto
for their unconditional
love and support.

ACKNOWLEDGEMENTS

First, I want to express my gratitude to Dr. David Suleiman for his trust, support and valuable guidance, which made possible the successful completion of this goal. I appreciate his advice during this journey and contribution to my professional and personal development. I would like to express my sincere thanks to the members of my graduate committee: Dr. Agnes Padovani, Dr. L. Antonio Estévez, Dr. María Curet for their advice and suggestions to this dissertation, that was performed with the financial support of the National Science Foundation through grant No. HRD-0833112 (UPRM-CREST Program) and grant No. HRD-0832961 (PRLSAMP - BD Program).

I extend my gratitude to Prof. Marcelo Suárez, director and IRG4 Leader of the UPRM-CREST Program, for his support and encouragement to participate in outreach educational activities and scientific conferences, and to Norma Gómez for her assistance in administrative processes. I also like to acknowledge the support of Prof. Danilo C. Pozzo and the graduate students Mónica Ospinal and Pablo de la Iglesia, of the University of Washington, where the SAXS experiments were conducted; Prof. Carlos Rinaldi, Prof. Oscar Perales, Jeremiah Hubbard and Boris Renteria, of the University of Puerto Rico at Mayagüez, for the FTIR facilities; Prof. Yossef Elabd and the graduate students Holly Salerno and Francis Richey, of Drexel University for the EIS facilities; Prof. John Staser, of Ohio University, for the tutoring and technical support with the EIS measurements; and Scott Brasswell of the Nanotechnology User Facility of the University of Washington (member of the National Nanotechnology Infrastructure Network) for the use of the TEM.

I would like to acknowledge the technical guidance of Ángel Zapata and the support of the administrative personnel of the Chemical Engineering Department especially to the graduate student counselor, Waleska Velázquez.

I also want to thank my labmates Edward Guerrero, Ariangelis Ortiz, Noelia Lasanta, and Maritza Pérez who shared with me this journey turning from colleagues into friends. I sincerely acknowledge the help and support of all the undergraduate students

who collaborated in this project during the past years, especially Stephanie Ortiz, Emanuel Sánchez, Eva González, Ishar Rosado, Nelson Rodríguez, Luis G. Rivera, Pablo Valero, and Bryan Sánchez.

I extend my gratitude to the Educational and Outreach Program of the Engineer Research Center for Structured Organic Particulate Systems (ERC-SOPS), especially to professors Carlos Velázquez and Nelson Cardona for sharing their passion for education by giving me the opportunity and trust to collaborate in this program and help me to grow and develop as an educator. I am grateful of the administrative officers, Carmen V. Santiago and Katherine Pérez, for their administrative assistance and unconditional support to all the academic and extracurricular activities. Also I would like to thanks the pillars and other *founders* of the program Daniel Mateo, Miguel Florián and David Mota for sharing with me their knowledge in pharmaceutical engineering and give me the opportunity of been part of such an amazing work group, that promoted the growth of a beautiful and sincere friendship.

My deepest gratitude to my parents, José L. Avilés and Sonia M. Barreto, who gave me the strongest support and unconditional love and teach me the importance of education and moral values. To my sister Sully Mar Avilés, my role model, for always trusting me and be by my side encouraging me to pursue my goals and helping me keep strong in hard times. To my brother-in-law and friend Jorge Torres for his love and support to my family. To the Muñiz-Barreto family, especially my cousins Mayra Muñiz, Marisel Muñiz and Celmarie Muñiz, for always being by my parent's side offering them assistance, company and love. To my godmother Célida Vale for sharing her passion about sciences and teach me the basis of chemistry. To Luz Barreto and the Barreto-Vale, Barreto-Rosa, Barreto-Acevedo, and Díaz-Barreto families for being part of my life and their unconditional support.

I am deeply grateful to my love, friend, counselor, and study partner David Mota for being my inspiration, support, and guide through this path and my life. Also thanks for helping me to discover myself and always push me to be a better person and professional.

Finally, I like to thank my friends: Keren Valentín, Isaac Torres, Darlene Galloza, Marlene Galloza, Karem Court, Liliana Gámez, Angélica Román, Christian Rivera, Stephany Herrera, Camilo Mora, Eduardo Ruiz, Paul Meza, Lorena Maldonado, Madeline Candelaria, Vladimir Villanueva, Argenis López, Ana Arévalo, José Roberto Ramírez, Mauricio León, Vivian Florián, Leonel Quiñones, Karl Pellicier, Julio Echevarría, Darwin Santana, Angie Hernández, and Imiraily Hernández for the moments we shared and their support through this journey.

TABLE OF CONTENTS

LIST OF TABLES

LIST OF FIGURES

LIST OF APPENDICES

CHAPTER 1

INTRODUCTION

1.1. Fuel Cells

Since 1960, fuel cells have been acquiring attention as an alternative power source, due to their high energy density and efficiency, low pollution and wide applications [1,2]. There are two main types of fuel cells, *proton exchange membrane fuel cells (PEMFC) and direct methanol fuel cells (DMFC)*. In general a fuel cell is an electrochemical device that is fed of a fuel (hydrogen in PEMFC or methanol in DMFC) that is oxidized at the anode, and oxygen or air that is reduced at the cathode. The protons released during the oxidation of the fuel are conducted through a proton exchange membrane (PEM) to the cathode. Since the membrane is not electrically conductive, the electrons released from hydrogen travel along the electrical detour provided using a conductor and an electrical current is generated, as shown in the diagram of Figure 1.1.

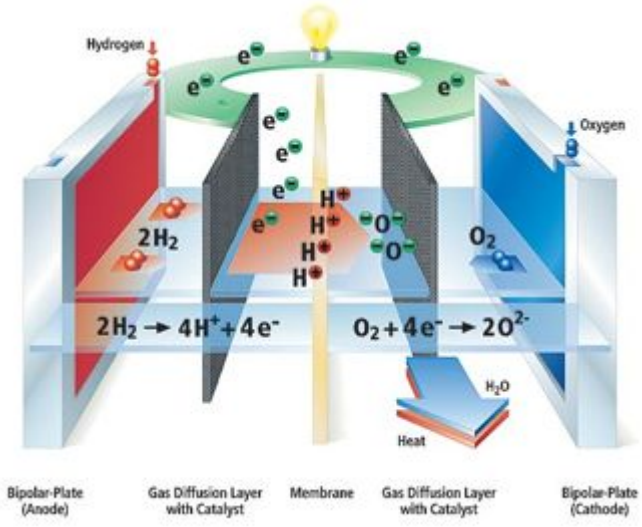

Figure 1.1. Schematic diagram of a PEMFC [3]

In the center of the fuel cell is the membrane electrode assembly (MEA). The MEA consists of the PEM, catalyst and gas diffusion layers (GDL). Typically, these components are individually fabricated. The conventional catalyst configuration consists of platinum (Pt) loadings of approximately 0.4 mg/cm^2 and the GDL of carbon paper or carbon cloth [4], that ensures that reactants effectively diffuse to the catalyst layer. The electrochemical reaction occurs at the interface of the GDL with the catalyst, as shown in Figure 1.1 [5].

The membrane is a fundamental component in the efficiency of the fuel cell. The two primary measures of the membrane performance are the membrane *permeability* (i.e., productivity) of the desired penetrant (in the case of protons is called proton conductivity) and the membrane *selectivity* (i.e., separation effectiveness) between penetrants and undesired fuel permeation. In order to measure the selectivity of a PEM its transport properties, (i.e. proton conductivity and fuel permeability) have to be studied. Proton conductivity is the ability to conduct protons through the membrane and is intimately connected with both acid and water (i.e. ionomer hydration) content of the membrane. This conductivity is affected by the strength of the acid, the chemical structure and morphology of the membrane, as well as temperature [6]. Fuel permeability refers to the passage of unreacted fuel through the PEM.

In the case of DMFC, current PEM have high methanol permeation rates. For this case, a membrane with the property of blocking a highly concentrated methanol solution is required [5]. Previous studies have found that a polymer that includes on its structure non-ionic blocks are highly potential, since the non-ionic domains could be designed to be effective barriers for methanol [7].

Since the stability of membranes against thermo-mechanical and chemical stresses is also an important factor in determining both their short- and long-term performance, additional characterization is required. A combination of chemical, thermal and X-ray techniques are used to elucidate the nanostructure of the membranes and explain the transport properties and fuel mechanisms for an effective PEM performance.

1.2. Specialty Separations

The selective separations of some substances mixture are difficult to achieve due their similarity in thermal and molecular properties such as vapor pressure, boiling point and molecular size. For these separations, membrane technology is widely used. Membrane technology is a low energy consuming technology that offers process simplicity, effectiveness, efficiency and economic benefits for specific separations or removal of undesirable components [8]. Some membrane separation processes include gas separation, pervaporation, osmosis, electrodialysis, ultrafiltration and nanofiltration [9–12].

Among the gas separation processes an application that is receiving widely attention since the 911 and anthrax terrorist attacks to the US and the recently Syrian chemical weapon attack is the development of chemical and biological protective clothing (CBPC). The chemical warfare agents (CWA) most commonly used are nerve agents, as Agent Orange and Sarin, that operate by blocking neurochemical pathways in humans, can lead to loss of autonomic functions (e.g., breathing) and muscle control [13,14]. Since these chemical warfare agents are highly toxic and can penetrate the skin rapidly, effective individual protection against exposure is of great importance in the military and in civilian defense [15].

CBPC need to provide the necessary protection against threat agents, block their passage, but also be comfortable to wearers allowing water vapor breathability, as shown in Figure 1.2. Cross-linked butyl rubber or polyethylene with activated charcoal or carbon pellets were used for this application but the combination of heavy and impermeable protective materials negatively impacted the users' performance [16–18]. CBPC increases the heat stress on the body and cause fatigue problems due to the heavy workload and with prolonged use because of the lack of water vapor evaporation for personal cooling reducing task efficiency and the individual's range of motion [19]. The commonly accepted as the desired range for water vapor transport rate (VTR) in CBPC is 1500–2000 g/m^2day^1 [15].

Many polymeric materials have been proposed for dealing with the challenges of increasing breathability while maintaining high levels of protection. Among them the study of hydrophilic membranes such as PEM with sulfonic groups attached to their backbone has gain attention. The hydrophilic region formed by sulfonic acid groups promotes water transport and

provides effective barrier to organic compounds, which are desirable for chemical protection application [16,20,21].

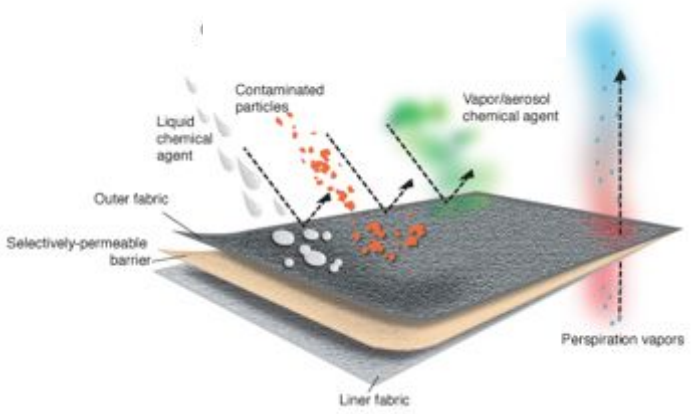

Figure 1.2. Schematic diagram of CBPC [22]

1.3. Proton Exchange Membranes (PEM)

A PEM is a semipermeable solid polymer electrolyte made of ionomers, which has the ability of transferring protons in moist state, and is impermeable to some compounds (e.g. oxygen and methanol). PEMs contain negatively charged groups, such as $–SO_3^-$, PO_3^{2-} or $-PO_3H^-$ [23] fixed to the membrane backbone designed to work as a barrier that only allows the conduction of protons or compounds with high chemical affinity (i.e. water).

The most commonly used PEM is Nafion® [7,24,25]. This perfluorosulfonic PEM has high proton conductivity and good mechanical and thermal stability [26–29], but it has several disadvantages, such as poor selectivity, high methanol permeation rates, limited processability due to the perfluorinated segments and high cost.

A variety of polymers have been studied in order to develop membranes that overcome the disadvantages and limitations of current commercial PEMs. A list of some potential materials is shown in Table 1.1.

Table 1.1. Some PEM materials studied for fuel cell and separation applications.

Material	Reference
poly(styrenesulfonic acid) (PSSA)	[30]
sulfonated tetrafluoroethylene (Nafion®)	[31]
sulfonated phenol-formaldehyde	[30]
sulfonated polyphosphazene	[32]
sulfonated poly(phenylene oxide)	[33]
sulfonated polyarylene ether sulfone	[34]
sulfonated polyetherketone	[35]
sulfonated poly[bis(3-methylphenoxy) phosphazene	[32]
acid-doped poly(benzimidazole)	[36]
sulfonated poly(4-vinylpyridinium-styrene-4-vinylpyridinim)	[37]
sulfonated poly(styrene-(ethylene-co-butylene)-styrene)	[38]
poly(vinylidene fluoride-hexafluoropropylene) (PVDF-HFP)	[39]
poly(ether ketone ketone)	[40]
sulfonated poly(ethylene-alt-tetrafluoro- ethylene)	[41]
poly(benzimida-zole)	[41]
poly (2,6-dimethyl-1,4-phenylene oxide)	[23]
phosphoric acid-doped polybenzimidazole (PBI/H_3PO_4)	[23]
polyethersulfone	[42]
sulfonated poly(styrene-isobutylene-styrene)	[7]
polystyrene-ethylene-butylene-polystyrene	[43]
poly(tetrafluoroethylene)-G-polystyrene sulfonic acid	[44]
poly(tetrafluoro-co-hexafluoropropylene)-G-polystyrene sulfonic acid	[44]
sulfonated phthalic polyimide	[44]
sulfonated poly(phenylqunoxaline)	[44]
sulfonated poly(2,6-diphenyl 1-4,phynylen oxide)	[44]
benzylsulfonate-G-polybenzimidazoles	[44]
Pphosphoric acid doped poly(ethylene oxide)-(PEO/H3PO4)	[44]
poly(ethyleneimine)-(BPEI/H3PO4/H2SO4/HCl)	[44]
sulfonated polyethersulfone doped polybenzimidazoles (S-PSU/PBI)	[44]
poly(trifluorostyrene sulfonic acid)	[44]
poly(phenylene sulfide)	[42]
propane sulfonated poly(p-phenylene terephthalamide) (PPTA-PS)	[44]

1.4. Justification and Dissertation Overview

Disadvantages of current PEM's are one of the most important constrains that limit the industrial production and commercialization of fuel cells. While security and protection are two critical challenges for people in general and in particular for the military forces, the development and implementation of new and more efficient alternatives for chemical and biological protective clothing (CBPC) is of outmost importance. To develop an efficient PEM for these applications, some requirements like high proton transport, low methanol permeability, high selectivity and separation efficiency need special attention.

PEM with hydrophilic groups are promising materials to meet these requirements. Among the variety of polymers that have been studied and characterized to explore their transport properties, block copolymers that combine ionic and non-ionic domains have gained our attention, especially the ones with a polystyrene block (PS). Polystyrene has been known for years as a commodity plastic with excellent chemical resistance, good environmental stress crack resistance, easy processability, and moderate cost [45]. PS has an aromatic ring on its backbone that can be easily functionalized with sulfonic groups (SO_3^-) using aromatic electrophilic substitution to create an ionomeric polymer.

Block copolymers composed of sulfonated polystyrene and a non-ionic elastomeric block like could present good transport and barrier properties. From the list in Table 1.1, the transport properties of sulfonated poly(styrene-isobutylene-styrene) (SIBS) have been widely studied at low sulfonation levels for fuel cells and CBPC applications giving good transport properties [24,46,47].

SIBS is a tri-block copolymer that presents morphological changes at the nanoscale upon sulfonation. Its chemical structure after sulfonation using acetyl sulfate is shown in Figure 1.3, where the sulfonic acid groups bound to the para- configuration of the polystyrene aromatic ring. Since these hydrophilic groups promote the proton transport, high sulfonation levels and the addition of other hydrophilic functionalization were areas that required attention as they could lead to an improvement of the transport properties and an increase of the selectivity and efficiency of sulfonated SIBS.

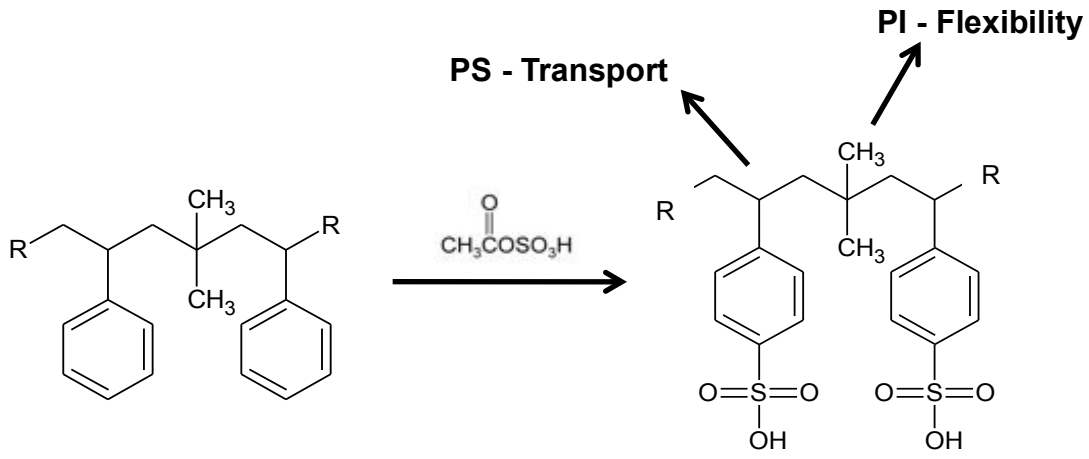

Figure 1.3. Sulfonation reaction and chemical structure of sulfonated SIBS

This research evaluated changes in poly(styrene-isobutylene-styrene) with respect to some major variables. First, the effect of sulfonation level and counter ion substitution was studied in Chapter 2 to determine the influence of increasing the ionic domains and hydration on the properties of SIBS. Then, Chapter 2 focuses on the incorporation of single-walled carbon nanotubes at different loadings and with different types of chemical functionalizations to understand the effect of physical and chemical modifications. Finally, in Chapter 4 blends of SIBS and another polymer, poly(styrene-isoprene) (SI), were studied to investigate the impact of morphology. Since both applications require resistance to organics, while still providing high transport of protons (fuel cells) and water (breathable clothing), our research was focused on developing PEM's with high selectivity to enhance the performance of current DMFC and increase the efficiency of specialty separations (i.e., chemical and biological protective clothing). The transport properties and the influence of water and morphology of the resulting PEM's have been evaluated for each application and the results obtained have been explained using an in-depth materials characterization approach.

1.5. References

[1] X. Yuan, H. Wang, J. Colinsun, J. Zhang, AC impedance technique in PEM fuel cell diagnosis—A review, Int. J. Hydrogen Energy. 32 (2007) 4365–4380.

[2] H. Tang, S. Wang, M. Pan, S.P. Jiang, Y. Ruan, Performance of direct methanol fuel cells prepared by hot-pressed MEA and catalyst-coated membrane (CCM), Electrochim. Acta. 52 (2007) 3714–3718.

[3] PEMFC Single Cell, (2007).

[4] S. Litster, G. McLean, PEM fuel cell electrodes, J. Power Sources. 130 (2004) 61–76.

[5] H. Chang, J.R. Kim, J.H. Cho, H.K. Kim, K.H. Choi, Materials and processes for small fuel cells, Solid State Ionics. 148 (2002) 601–606.

[6] T. Peckham, Y. Yang, S. Holdcroft, Proton Exchange Membranes, in: Prot. Exch. Membr. Fuel Cells, CRC Press, 2009.

[7] Y.A. Elabd, E. Napadensky, J.M. Sloan, D.M. Crawford, C.W. Walker, Triblock copolymer ionomer membranes. Part I. Methanol and Proton Transport, J. Memb. Sci. 217 (2003) 227–242.

[8] S.S. Hosseini, M.R. Omidkhah, A. Zarringhalam Moghaddam, V. Pirouzfar, W.B. Krantz, N.R. Tan, Enhancing the properties and gas separation performance of PBI–polyimides blend carbon molecular sieve membranes via optimization of the pyrolysis process, Sep. Purif. Technol. 122 (2014) 278–289.

[9] M.A. Aroon, A.F. Ismail, T. Matsuura, M.M. Montazer-Rahmati, Performance studies of mixed matrix membranes for gas separation: A review, Sep. Purif. Technol. 75 (2010) 229–242.

[10] X. Ruan, G. He, B. Li, X. Yan, Y. Dai, Chemical potential analysis for directing the optimal design of gas membrane separation frameworks, Chem. Eng. Sci. 107 (2014) 245–255.

[11] P. Luis, J. Degrève, B. Van der Bruggen, Separation of methanol–n-butyl acetate mixtures by pervaporation: Potential of 10 commercial membranes, J. Memb. Sci. 429 (2013) 1–12.

[12] P.H.H. Duong, T.-S. Chung, Application of thin film composite membranes with forward osmosis technology for the separation of emulsified oil–water, J. Memb. Sci. 452 (2014) 117–126.

[13] N.J. Choi, J.-H. Kwak, Y.-T. Lim, T.-H. Bahn, K.-Y. Yun, J.-C. Kim, et al., Classification of chemical warfare agents using thick film gas sensor array, Sensors Actuators B Chem. 108 (2005) 298–304.

[14] Y. Wang, Z. Zhou, Z. Yang, X. Chen, D. Xu, Y. Zhang, Gas sensors based on deposited single-walled carbon nanotube networks for DMMP detection., Nanotechnology. 20 (2009) 345502.

[15] X. Lu, V. Nguyen, X. Zeng, B.J. Elliott, D.L. Gin, Selective rejection of a water-soluble nerve agent stimulant using a nanoporous lyotropic liquid crystal–butyl rubber vapor barrier material: Evidence for a molecular size-discrimination mechanism, J. Memb. Sci. 318 (2008) 397–404.

[16] K.H. Jung, B. Pourdeyhimi, X. Zhang, Chemical protection performance of polystyrene sulfonic acid-filled polypropylene nonwoven membranes, J. Memb. Sci. 362 (2010) 137–142.

[17] L. Szinicz, History of chemical and biological warfare agents, Toxicology. 214 (2005) 167–181.

[18] X. Hao, J. Zhang, Y. Guo, Study of new protective clothing against SARS using semi-permeable PTFE/PU membrane, Eur. Polym. J. 40 (2004) 673–678.

[19] S.L. Murray, Y.L. Simon, H. Sheng, The effects of chemical protective suits on human performance, J. Loss Prev. Process Ind. 24 (2011) 774–779.

[20] H.H. Schwarz, G. Malsch, Polyelectrolyte membranes for aromatic–aliphatic hydrocarbon separation by pervaporation, J. Memb. Sci. 247 (2005) 143–152.

[21] S.M. Avilés-Barreto, D. Suleiman, Synthesis and characterization of sulfonated poly(styrene-isoprene-styrene): Effects of linear vs. branched morphology and counter-ion substitution, J. Memb. Sci. 362 (2010) 471–477.

[22] Blauer Manufacturing Co., Inc., (n.d.).

[23] S.J. Peighambardoust, S. Rowshanzamir, M. Amjadi, Review of the proton exchange membranes for fuel cell applications, Int. J. Hydrogen Energy. 35 (2010) 9349–9384.

[24] D. Suleiman, Y. a. Elabd, E. Napadensky, J.M. Sloan, D.M. Crawford, Thermogravimetric characterization of sulfonated poly(styrene-isobutylene-styrene) block copolymers: effects of processing conditions, Thermochim. Acta. 430 (2005) 149–154.

[25] X. Lu, S. Wu, L. Wang, Z. Su, Solid-state amperometric hydrogen sensor based on polymer electrolyte membrane fuel cell, Sensors Actuators B Chem. 107 (2005) 812–817.

[26] L.A. Diaz, G.C. Abuin, H.R. Corti, Methanol sorption and permeability in Nafion and acid-doped PBI and ABPBI membranes, J. Memb. Sci. 411-412 (2012) 35–44.

[27] Q. Duan, H. Wang, J. Benziger, Transport of liquid water through Nafion membranes, J. Memb. Sci. 392-393 (2012) 88–94.

[28] H. Tang, S. Peikang, S.P. Jiang, F. Wang, M. Pan, A degradation study of Nafion proton exchange membrane of PEM fuel cells, J. Power Sources. 170 (2007) 85–92.

[29] Y. Zhao, J. Yin, Synthesis and properties of poly(ether ether ketone)-block-sulfonated polybutadiene copolymers for PEM applications, Eur. Polym. J. 46 (2010) 592–601.

[30] W. Vielstich, A. Lamm, H.A. Gasteiger, Handbook of Fuel Cells: Fundamentals, Technology and Applications, Wiley & Sons Ltd., Chichester, England, 2003.

[31] E. Chen, History, in: Fuel Cell Technol. Handb., CRC Press, 2002.

[32] Q. Guo, P. N. Pintauro, H. Tang, S. O'Connor, Sulfonated and crosslinked polyphosphazene-based proton-exchange membranes, J. Memb. Sci. 154 (1999) 175–181.

[33] B. Vishnupriya, K. Ramya, K.S. Dhathathreyan, Synthesis and characterization of sulfonated poly(phenylene oxides) as membranes for polymer electrolyte membrane fuel cells, J. Appl. Polym. Sci. 83 (2002) 1792–1798.

[34] X. Zhang, S. Liu, J. Yin, Synthesis and characterization of a new block copolymer for proton exchange membrane, J. Memb. Sci. 258 (2005) 78–84.

[35] C. Manea, M. Mulder, Characterization of polymer blends of polyethersulfone/sulfonated polysulfone and polyethersulfone/sulfonated polyetheretherketone for direct methanol fuel cell applications, J. Memb. Sci. 206 (2002) 443–453.

[36] J.T. Wang, J.S. Wainright, R.F. Savinell, M. Litt, A direct methanol fuel cell using acid-doped polybenzimidazole as polymer electrolyte, J. Appl. Electrochem. 26 (n.d.) 751–756.

[37] J.P. Gouin, C.E. Williams, A. Eisenberg, Microphase structure of block ionomers. 1. Study of molded styrene-4-vinylpyridinium ABA blocks by SAXS and SANS, Macromolecules. 22 (1989) 4573–4578.

[38] R.A. Weiss, A. Sen, C.L. Willis, L.A. Pottick, Block copolymer ionomers: 1. Synthesis and physical properties of sulphonated poly(styrene-ethylene/butylene-styrene), Polymer (Guildf). 32 (1991) 1867–1874.

[39] J. Fuller, A.C. Breda, R.T. Carlin, Ionic Liquid–Polymer Gel Electrolytes, J. Electrochem. Soc. 144 (1997) L67–L70.

[40] J.V. Gasa, R. a. Weiss, M.T. Shaw, Ionic crosslinking of ionomer polymer electrolyte membranes using barium cations, J. Memb. Sci. 304 (2007) 173–180.

[41] V. Neburchilov, J. Martin, H. Wang, J. Zhang, A review of polymer electrolyte membranes for direct methanol fuel cells, J. Power Sources. 169 (2007) 221–238.

[42] Z. Bai, M. Durstock, T. Dang, Proton conductivity and properties of sulfonated polyarylenethioether sulfones as proton exchange membranes in fuel cells, J. Memb. Sci. 281 (2006) 508–516.

[43] S. Elamathi, G. Nithyakalyani, D. Sangeetha, S. Ravichandran, Preparation and evaluation of ionomeric membranes based on sulfonated-poly (styrene_isobutylene_styrene) membranes for proton exchange membrane fuel cells (PEMFC), Ionics (Kiel). 14 (2007) 377–385.

[44] V. Mehta, J.S. Cooper, Review and analysis of PEM fuel cell design and manufacturing, J. Power Sources. 114 (2003) 32–53.

[45] P. Raghu, C.K. Nere, R.N. Jagtap, Effect of styrene–isoprene–styrene, styrene–butadiene–styrene, and styrene–butadiene–rubber on the mechanical, thermal, rheological, and morphological properties of polypropylene/polystyrene blends, J. Appl. Polym. Sci. 88 (2003) 266–277.

[46] Y.A. Elabd, E. Napadensky, Sulfonation and characterization of poly(styrene-isobutylene-styrene) triblock copolymers at high ion-exchange capacities, Polymer (Guildf). 45 (2004) 3037–3043.

[47] J.S. Lawton, D.E. Budil, Spin Probe ESR Study of Cation Effects on Methanol and DMMP Solvation in Sulfonated Poly(styrene−isobutylene−styrene) Triblock Copolymers at High Ion-Exchange Capacities, Macromolecules. 43 (2010) 652–661.

CHAPTER 2

TRANSPORT PROPERTIES OF SULFONATED POLY(STYRENE-ISOBUTYLENE-STYRENE) MEMBRANES WITH COUNTER-ION SUBSTITUTION

2.1. Abstract

In this study, the transport properties of poly(styrene-isobutylene-styrene) (SIBS) were determined as a function of sulfonation level (0-94.9%) and counter ion substitution (Ba^{+2}, Ca^{+2}, Mg^{+2}, Mn^{+2}, Cu^{+2}, K^{+1}) for fuel cell and chemical and biological protective clothing (CBPC) applications. Increasing the sulfonation level improved the ion exchange capacity (IEC) of the membranes up to a maximum (1.71 mequiv/g), suggesting a complex 3-D network at high sulfonation levels. Results show that proton conductivity increases with IEC and is very sensitive to hydration levels. Methanol permeability, although also sensitive to IEC, shows a different behavior than proton conductivity, suggesting fundamental differences in their transport mechanism. The incorporation of counter ion substitution decreases both methanol and proton transport. Methanol permeability seems to be related to the size of the counter-ion studied, while proton conductivity is more sensitive to water contents, which is also reduced upon the incorporation of counter-ions. To complement the studies, selectivity (i.e., proton conductivity/methanol permeability) of the studied membranes was determined and compared to Nafion® 117. The efficiency of the membranes to separate DMMP and water also show high selectivity values for the sulfonated membranes (up to 8.55). Gas phase permeability studies for CBPC applications also showed strong sensitivity to IEC.

2.2. Introduction

Many applications for proton exchange membranes (PEM's) are known, especially in the area of electrochemical and energy efficient devices such as fuel cells [1-6]. As mentioned in Chapter 1, the most commonly used PEM is Nafion® [1–6]. Even though it has a high proton conductivity and good mechanical and thermal properties [5–8], it has several disadvantages limiting the performance of existing devices.

To meet the requirements of high ionic conductivity with proper chemical, thermal and mechanical strength and to overcome the transport issues, a variety of block copolymers have been studied and characterized to explore their properties [9–11]. They can be grouped into: perfluorinated ionomeric membranes (e.g., Nafion®, Flemion®, polyvinylidene fluoride-hexafluoropropylene), non-fluorinated hydrocarbons (aliphatic and aromatic) ionomeric membranes (e.g., polystyrenesulfonic acid, sulfonated polystyrene-ethylene-butylene-polystyrene, sulfonated polyphenylene oxide, sulfonated polyetherketoneketone), and acid-base complexes (e.g., phosphoric acid-doped polybenzimidazole)) [1,4,9,10,12–16].

Hydrocarbon polymers containing polar groups, as sulfonic groups (-SO_3-), which retain high amounts of water over a wide temperature range are particularly attractive and relatively cheaper to synthesize than perfluorinated polymers [16,17]. Sulfonic groups can be added to hydrocarbon polymers that have an aromatic ring on their backbone by post-sulfonation using aromatic electrophilic substitution. Incorporation of this sulfonic groups increases properties like strength, hydrophilicity, and proton conductivity [18,19]. Sulfonated copolymers, with an elastomeric block, have gained interest because they combine properties of two materials and have a highly ordered sequence of both ionic and non-ionic blocks, since only one of the blocks is sulfonated [20]. On the ionic blocks phase segregation can occur due to the electrostatic interaction among ion pairs forming ion clusters. As the ionic domains increase, due to the increment of sulfonic groups, these clusters connect forming ionic channels that facilitate the transport of protons [1,18]. On the other hand, the non-ionic domains could be designed to be effective barriers for methanol (MeOH) [1].

Previous studies have characterized sulfonated poly(styrene-isobutylene-styrene) (SIBS) and evaluated their potential as a viable PEM for fuel cells and protective clothing applications [2,18,21]. SIBS is a tri-block thermoplastic elastomer which is composed of glassy outer blocks (polystyrene) and rubbery inner blocks (poly(isobutylene)) [22,23]. By sulfonating the polystyrene blocks, an ionomer that self assembles into a three-phase nanostructured morphology in the solid state and a polymer that combines ionic and non-ionic properties can be produced [24]. To increase its selectivity ionic cross-linking is suggested. One approach is to exchange with cations some of the protons in the acidic membranes. The cation-substituted membrane produced by the exchange reaction should have low water solubility and form a stable crosslink that can enhance properties as transition temperatures, plateau modulus and tensile strength. Also, it can reduce the solvent swelling and methanol permeability [14]. This study presents the synthesis and characterization of poly(styrene-isobutylene-styrene) with respect to two major variables: sulfonation level and counter ion substitution. The transport properties of the resulting PEM's have been evaluated and the results have been explained using an in-depth materials characterization approach.

2.3. Experimental Methods

2.3.1. Materials

Poly(styrene-isobutylene-styrene) (SIBS) was purchased from Kaneka® with properties of 30 wt.% polystyrene and a molecular weight of 65,000 g/mol. Other chemicals used include: methylene chloride (Fisher Scientific, 99.8%), sulfuric acid (Sigma Aldrich, 95-98%), acetic anhydride (Aldrich Chemical, 99+%), toluene (Fisher Scientific, 99.8%), hexyl alcohol (Aldrich Chemical, 98%), methanol (Fisher Scientific, 99.9%), barium chloride (Sigma–Aldrich, anhydrous, powder, 99.99%), calcium chloride (Sigma–Aldrich, anhydrous, powder, 99.99%), magnesium chloride (Sigma–Aldrich, anhydrous, powder, 99.99%), manganese chloride ($MnCl_2$) (Acros Organics, 99+%), copper (II) chloride ($CuCl_2$) (Across Organics, anhydrous, 99%), potassium chloride (KCl) (Fisher Scientific), and deionized water. All chemicals were used without further purification.

2.3.2. Polymer Sulfonation

The sulfonation of SIBS was performed using the suggested procedure of Elabd and Napadensky [1,18]. Some modifications were considered, an example of the sulfonation procedure is as follows: a 10% (wt./v) solution of SIBS (30 g dried for 24 h at 60℃) in methylene chloride was prepared. The sulfonating agent, acetyl sulfate, in methylene chloride is prepared by cooling 200 ml of methylene chloride in an ice bath for 10 min, and then acetic anhydride is added to the methylene chloride under stirring conditions. The cooling is to account for the exothermic heat of reaction, while avoiding solvent evaporation. Sulfuric acid is added 10 min after the acetic anhydride with an acetic anhydride mole ratio of 1:1. The sulfonating agent was slowly added to the polymer solution to begin the sulfonation reaction. The reaction was terminated after 24 h by adding 200 ml of methanol and the solvents were allowed to evaporate at room temperature for 5 days. The reacted polymer was washed several times with deionized water until the pH of the water was neutral. The used water with residual acetyl sulfate was neutralized with sodium hydroxide to minimize the waste produced in this process. Since the concentration of acetic acid produced after neutralization is lower than the allowed disposable limit, the neutralized water was safe to discard. The polymer was then dried at 60℃ for 48 h. The sulfonation procedure was repeated several times with different amounts of acetyl sulfate to obtain various sulfonating levels. Higher sulfonation levels require a larger excess of the sulfonation agent since, upon sulfonation, ionic nanochannels are formed and it is difficult to overcome the mass-transport limitations to reach the last unoccupied sites available for sulfonation.

2.3.3. Membrane Casting

Once sulfonated, SIBS was pH balanced and dry, it was dissolved in a solution (85/15) (v/v) of toluene and hexyl alcohol with a polymer concentration of 5 wt. %. SIBS membranes were solvent cast in Teflon® Petri dishes for one week at room temperature allowing for the membranes to thermodynamically self-assemble as the solvent

evaporated. They were then dried at 60℃ for 24 h to remove the final residual solvent. The unsulfonated polymer was cast similarly, but with pure toluene instead.

2.3.4. Counter Ion Substitution

The membranes were neutralized by immersing the sulfonated membranes in acid form in 1.0 M solution of the salts containing the desired cation ($BaCl_2$, $CaCl_2$, $MgCl_2$, $MnCl_2$, $CuCl_2$, and KCl) for 24 h. The cation substitution takes place in a few minutes for thin membranes (e.g., 0.1 cm), but they were immersed for 24 h to allow for proper cation substitution. The cross-linked membranes were then washed using deionized water and dried in an oven at 60℃ for 24 h.

2.3.5. Nomenclature

The membranes were labeled SIBS-XX-Y^Z, indicating SIBS polymer followed by XX, which is the sulfonation mole percent obtained after elemental analysis (EA), Y, which is the cation substituted, and Z, which is the cation electrical charge before the substitution.

2.3.6. Materials Characterization

Elemental analysis was performed by Atlantic Microlab, Inc. in Norcross, GA to determine accurate sulfonation levels. Sulfonated membrane samples (1-3 mg) were analyzed for carbon, hydrogen and sulfur weight percent. Additional stoichiometric calculations were required to obtain the final mole percent of sulfonation for all the membranes studied.

Elemental Analysis, Inc. (Lexington, KY) performed the instrumental neutron activation analysis (INAA) to determine the amount of cations substituted. Cross-linked

membrane samples of approximately 0.1 g were analyzed for sulfur and cation composition. Results are presented as the mole ratio between cation and sulfonic groups.

Ion exchange capacity (IEC) was measured immersing 50 mg of the sulfonated membrane in a 1.0 M solution of NaCl for 24 hours. After removing the membrane, the solution was titrated using a 0.1 M solution of NaOH until the pH was neutral. The IEC was calculated from the moles of ion substituted divided by the initial dry mass of the membrane.

Fourier transform infrared spectroscopy (FT-IR) was used to confirm the presence of sulfonic groups and determine their aromatic substitution configuration. Infrared spectra of the samples were collected using a Varian 800 FTIR Scimitar Series Spectrometer and a ZnSe ATR holder with a wavenumber range of 600-4000 cm^{-1} using 100 scans at 8 cm^{-1} resolution.

The thermal stability and degradation temperatures of the samples were determined using a TGA/SDTA 851 from Mettler Toledo by heating the samples to 800℃ at a constant heating rate of 10℃/min under a nitrogen atmosphere.

To confirm the assignments of the degradation temperatures and determine the composition of the remaining mass, a TGA 2950 Thermogravimetrical Analyzer (TA Instruments) coupled to a Thermo Scientific TGA-FTIR interface was used under a helium atmosphere in a temperature range of 25 to 850℃ at a heating rate of 15℃/min. The gas cell temperature was set to 220℃ and the transfer line to 210℃.

Structure-property relations for dry sulfonated and counter-ion substituted membranes were determined using small-angle X-ray scattering (SAXS). The experiments were performed in the Chemical Engineering Department of the University of Washington, Seattle, using a one dimension SAXSess mc2 and SAXSquanTM-Software for the data analysis.

Transmission Electron Microscopy (TEM) was used to obtain an image of the polymer membrane upon sulfonation. The experiments were performed in the Nanotechnology User Facility of the University of Washington, Seattle, using a FEI

Tecnai G2 F20 TEM. The samples were spin-coated at 4000 rpm for one minute onto Carbon B copper grits (Ted Pella, Inc.).

Solvent swelling experiments were performed to determine absorption limitations and their effect on the membrane transport. For swelling measurements, square samples of the membranes were dried at 60℃ for 24 h, weighed and then immersed into vials containing deionized water. The weight of wet membranes was determined, after removing the surface solvent by blotting it with a tissue paper, at different times until equilibrium was reached.

In-plane ion conductivity for each membrane was measured using electrochemical impedance spectroscopy (EIS) over a frequency range of 0.1 Hz and 1MHz with an applied voltage of 10 mV (AC Solartron impedance system: 1260 impedance analyzer, 1287 electrochemical interface, Zplot software). Membranes were cut into 3 x 0.5 cm strips and submerged in deionized (DI) water for at least 24 h before the conductivity measurements were performed. The membrane strips were then loaded in hydrated form into an open cell consisting of four Pt parallel electrodes. Conductivities of the membranes were measured at room temperature (~25 °C), where the cell was filled with DI water to maintain full hydration of the membranes during the measurements. The real impedance was calculated from the *x*-intercept of the regression of Nyquist plot. In-plane conductivity, σ (S/cm), was calculated with Equation (2.1), where L_e is the distance between electrodes, R is the real impedance or resistance (Ω), and A is the cross sectional area. Wet membrane thickness and width were measured directly after the membrane was removed from the conductivity cell. The membrane thickness and width changed upon hydration and the changes varied with sulfonation level and counter-ion substitution; however, changes in width were more significant than changes in thickness. Additional details concerning the apparatus and procedures can be found elsewhere [25,26].

$$\sigma = \frac{L_e}{(AR)} \qquad (2.1)$$

Methanol permeability was measured at room temperature using a side-by-side diffusion cell. Membranes were prior hydrated with deionized water for 24 h and then put

between both sides of the cell, each one with a compartment of 0.3215 cm^2 of cross-sectional area. The donor compartment was filled with a 2.0 M MeOH solution and the receptor with deionized water. Infrared spectra from the receptor compartment were recorded every 10 min using 100 scans and 8 cm^{-1} resolution. The concentration of methanol was obtained by monitoring the C-O stretching of 1014 cm^{-1}. In addition, a GC-TCD (Shimadzu, GC-8) was used to corroborate the accuracy of the FT-IR technique. Methanol permeability was determined using the rearranged approximate solution of the continuity equation (2.2) for diffusion in plane sheet geometry (constant concentration in one side) [1,27], where C_A and C_B are the concentrations of methanol in the donor and receptor compartments, respectively, L is the membrane thickness (0.03 - 0.08 cm), V_B the volume of the receptor compartment (0.37 cm^3), A the cross-sectional area of the membrane (0.322 cm^2), D is the methanol diffusion coefficient (cm^2/s) and P the permeability (cm^2/s). The permeability represents the product of the diffusion coefficient times the solubility [27]. Permeability values were determined from the slope of $[(C_B(t)\, V_B\, L)/(C_A\, A)]$ versus time.

$$\frac{C_B(t)V_B L}{C_A A} = P\left(t - \frac{L^2}{6D}\right) \qquad (2.2)$$

Gas phase permeability experiments were performed using DMMP as a simulant of the chemical toxin Sarin, due to its similarity in chemical structure, physical properties and volatility [23]. The effective vapor permeability (P_{eff}) of water and DMMP through the membranes was studied at 37.5 ºC under a nitrogen atmosphere. Vials with a volume of 12 mL and an open top cap with a cross-sectional area of 6.08E-5 m^2 (hole diameter: 8.8 mm) were filled with 10 mL of permeant (i.e., water or DMMP). The membranes were previously cut, with an equal shape and size to that of the cap, and dried in a convection oven at 60 ºC for 24 h. The thickness of each precut membrane was measured with a digital caliper before it was place under the open cap. Vials where sealed with the cap and parafilm®, and its weight was measured using an analytical balance. Afterward the vials were placed in an oven and were weighed every 6 hours for 3 days.

Additional calculations were performed to obtain the effective vapor permeability for each permeant. First, the vapor transfer rate (VTR), which is the amount of permeant

that will flow through an area during a period of time, was obtained from the slope of the linear regression of the weight loss data vs. time. Using Fick's law and calculating the change in concentration using the ideal gas equation, the VTR (Appendix A) can be used to calculate the effective permeability through the membrane (cm^2/s) as shown in Equation (2.3):

$$P_{eff} = \frac{L\ x\ VRT}{P_i(MW_i/RT)} \qquad (2.3)$$

where L is the thickness of the membrane (cm), VTR is the vapor transfer rate (g/cm^2 s), P_i is the partial pressure of the permeant inside the vial (mm Hg) (for this experiment is equal to the permeant vapor pressure, P^{vap}), R is the universal gas constant (0.06236 m^3 mmHg / mol K), T is the experiment temperature (K) and MW_i is the permeant molecular weight (g/mol). The vapor pressure of DMMP was calculated using the Antoine coefficients determined by Butrow et al. [28], while the vapor pressure of water was calculated using the Antoine coefficients reported by Smith et al. [29].

2.4. Results and Discussion

2.4.1. Elemental Analysis

The sulfonation percent was calculated from the EA results of C H O S (Atlantic Microlab). The mole % sulfonation varied from 0 to 94.9% and as it will be explained ahead, FT-IR was used to confirm the location of the sulfonic groups in the polymer. INAA was used as an additional EA technique (Elemental Analysis Inc.) to confirm the consistency of the metal loading and to quantify the amount of cations in the polymer membranes. Table 2.1 shows the ratio of moles of metal per mole of sulfonic group in some of the polymer membranes studied. The results from Table 2.1 show two major effects: first, for each metal studied the mole ratio of metal to sulfonic group was very similar regardless of sulfonation level. Second, cations with a +2 charge have an average ratio of metal to sulfonic group that suggests one metal for every two sulfonic groups. For

the only cation with +1 charge studied (K^{+1}), the ratio of metal to sulfonic group suggests one mole of metal for each mole of sulfonic group.

Table 2.1. Counter-ion concentration in the crosslinked membranes by INNA.

	Cation mass fraction per sulfonic group					
Sample	**Ba^{+2}**	**Ca^{+2}**	**Mg^{+2}**	**Mn^{+2}**	**$Cu+^{2}$**	**K^{+1}**
SIBS 39 Ba	0.4235	0.4801	0.4900	0.4540	0.4100	0.8423
SIBS 63 Ba	0.3759	0.5667	0.4915	0.4525	0.4428	0.7245
SIBS 84 Ba	0.3595	0.5015	0.4947	0.4548	0.3657	0.9439

2.4.2. Ion Exchange Capacity

Ion exchange capacity (IEC) was measured for the sulfonated membranes and the results are presented in Table 2.2. The results suggest an optimum IEC with sulfonation level around 84.1% sulfonation. Beyond that sulfonation level the IEC is lower perhaps due to the formation of SO_2 bridges in the complex three-dimensional structure of the highly sulfonated polymer membranes.

Table 2.2. Sulfonation percentage and ion exchange capacity for sulfonated SIBS membranes.

Sample	**Sulfonation level (mol %)**	**IEC (mequiv./g)**
SIBS 29.7	29.7	0.77
SIBS 39.8	39.8	1.06
SIBS 63.1	63.1	1.69
SIBS 84.1	84.1	1.71
SIBS 92.0	92.0	1.57

2.4.3. Infrared Spectroscopy

Figure 2.1 shows the infrared spectra of sulfonated SIBS, where SIBS 0 represents the unsulfonated polymer and SIBS 94.9 the highest sulfonation level studied. The spectra for the sulfonated polymers show four additional bands (marked with +) at

high wavenumbers: 1151, 1124, 1034, 1007 cm^{-1}), representative of the stretching vibrations associated to the sulfonate group. The bands at 1034 and 1156 cm^{-1} represent the symmetric and asymmetric SO_2 stretch, respectively. While at lower wavenumbers shows two bands at 698 and 756 cm^{-1} (marked with +), that correspond to the mono-substitution of the aromatic ring, that move and lower their intensity as the sulfonation level increase and one at 830 cm^{-1} (also marked +), that confirms the para- substitution of the sulfonate group on the aromatic ring. Figure 2.2 shows the spectra of medium sulfonated counter-ion substituted membranes. The counter ion substitution increases the intensity of the bands and shifts the asymmetric S-O stretching vibrations bands towards a higher wavenumber suggesting that the cations are interacting with the sulfonic groups in a way that more energy is required to obtain this stretching vibration. This effect is the same for all cations although the shifts are unique for each cation, especially for the asymmetric S-O stretching at 1151 cm^{-1} (Table 2.3).

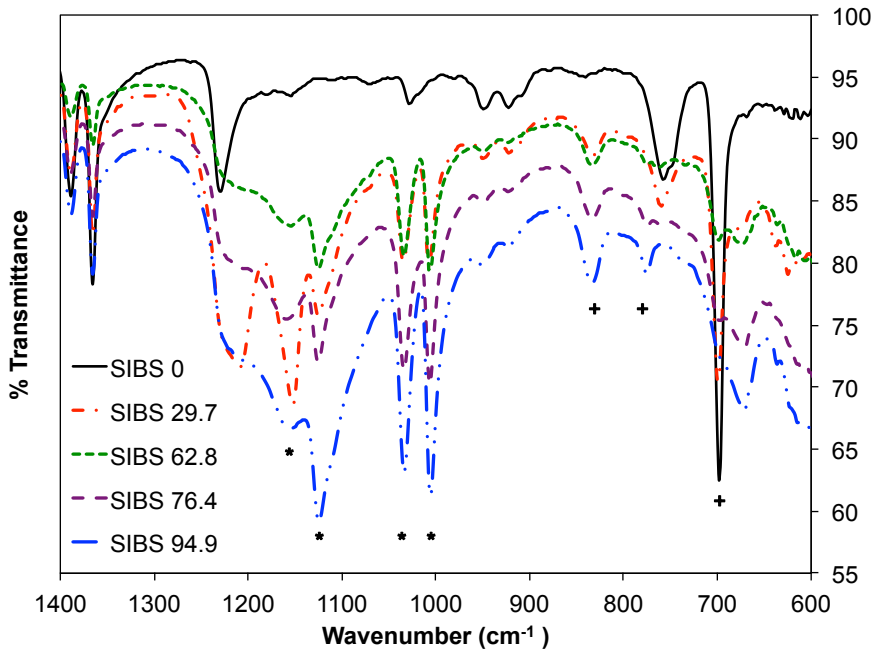

Figure 2.1. Infrared spectra of SIBS at various sulfonation levels (0, 29.7, 62.8, 76.4, and 94.9 mol%). The mark peaks represent stretching vibrations associated to sulfonated group (*) and the aromatic substitution (+).

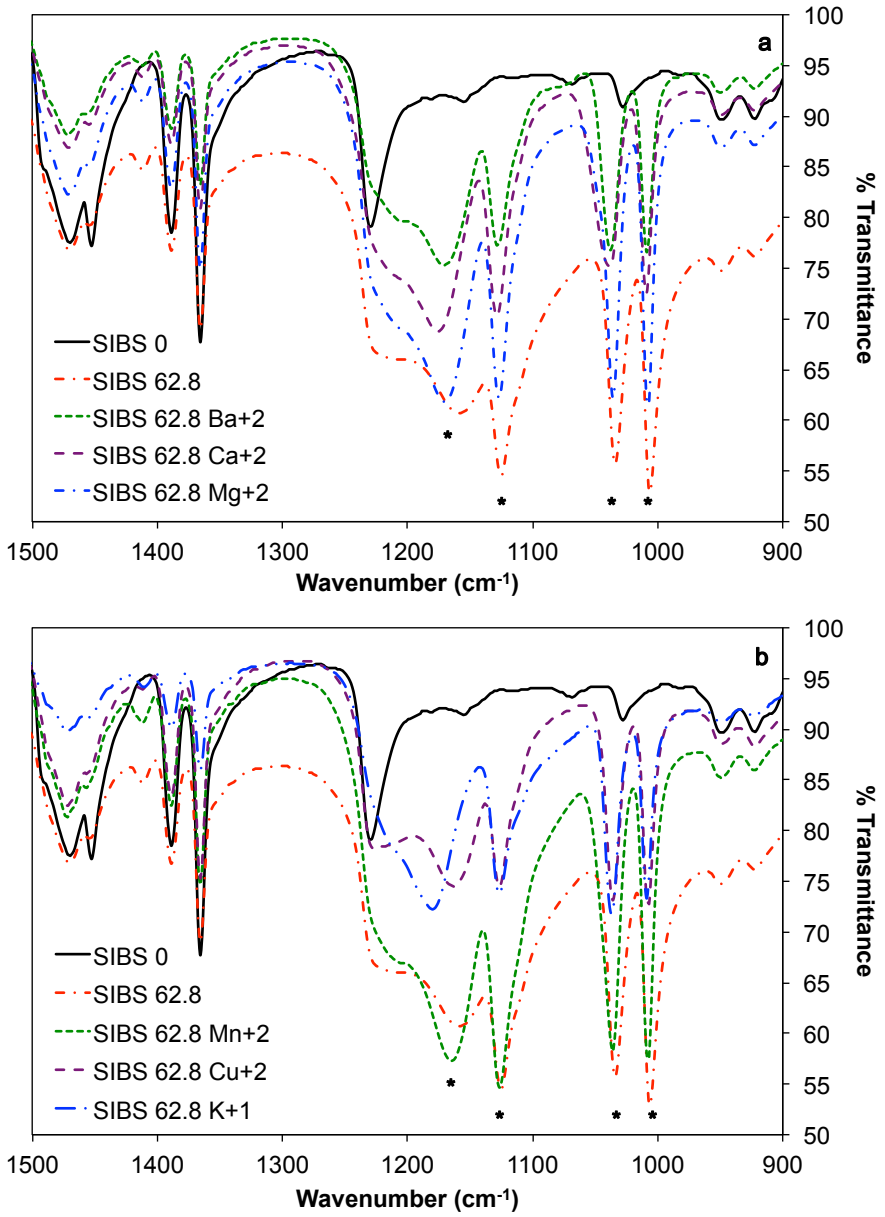

Figure 2.2. Infrared spectra of SIBS 62.8 cross-linked with various cations: a) Ba^{+2}, Ca^{+2}, Mg^{+2} and b) Mn^{+2}, Cu^{+2}, K^{+1}.

Table 2.3. FTIR stretching vibration bands for sulfonated and crosslinked SIBS membranes.

Sample	FTIR Stretching Bands (cm^{-1})			
SIBS 0	-	-	-	-
SIBS 29.7	1007	1034	1124	1151
SIBS 62.8	1007	1034	1124	1153
SIBS 76.4	1007	1034	1124	1159
SIBS 94.9	1007	1034	1124	1153
SIBS 29.7 Ba^{+2}	1009	1038	1126	1169
SIBS 62.8 Ba^{+2}	1009	1038	1128	1171
SIBS 94.9 Ba^{+2}	1009	1038	1128	1169
SIBS 29.7 Ca^{+2}	1009	1038	1128	1177
SIBS 62.8 Ca^{+2}	1009	1038	1128	1177
SIBS 94.9 Ca^{+2}	1009	1038	1128	1175
SIBS 29.7 Mg^{+2}	1009	1036	1126	1165
SIBS 62.8 Mg^{+2}	1009	1036	1126	1171
SIBS 94.9 Mg^{+2}	1009	1036	1126	1171
SIBS 29.7 Mn^{+2}	1009	1036	1126	1155
SIBS 62.8 Mn^{+2}	1009	1036	1126	1165
SIBS 94.9 Mn^{+2}	1007	1036	1126	1165
SIBS 29.7 Cu^{+2}	1009	1036	1124	1161
SIBS 62.8 Cu^{+2}	1007	1036	1126	1163
SIBS 94.9 Cu^{+2}	1007	1036	1126	1163
SIBS 29.7 K^{+1}	1009	1038	1126	1180
SIBS 62.8 K^{+1}	1009	1038	1126	1180
SIBS 94.9 K^{+1}	1009	1036	1126	1180

2.4.4. Thermogravimetrical Analysis

The thermogravimetrical analysis (TGA) for unsulfonated and sulfonated SIBS is presented in Figure 2.3 and Table 2.4. Upon sulfonation the degradation temperature of the polymer backbone increases from 365 ± 1 to 422 ± 2℃ regardless of sulfonation level. The TGA curves for the sulfonated SIBS show three weight loss stages, as it was demonstrated in previous studies [2,30].The first region (50- 200℃) is attributed to the atmospheric moisture absorbed by the hydroscopic ionic segments of the polymer and this region is left out of Table 2.4. The second (200-370℃) and third (370-430℃) are

attributed to the breakdown of the sulfonic groups attached to the styrene ring and the degradation of the polymer backbone, respectively (Table 2.4). In many studies of block copolymers the degradation of the polymer has two components, one for each block (one for polystyrene and another polyisobutylene). In this case only one band is observed for the degradation of the block copolymer. A previous study reports that these two bands may overlap and are indistinguishable from each other[30].

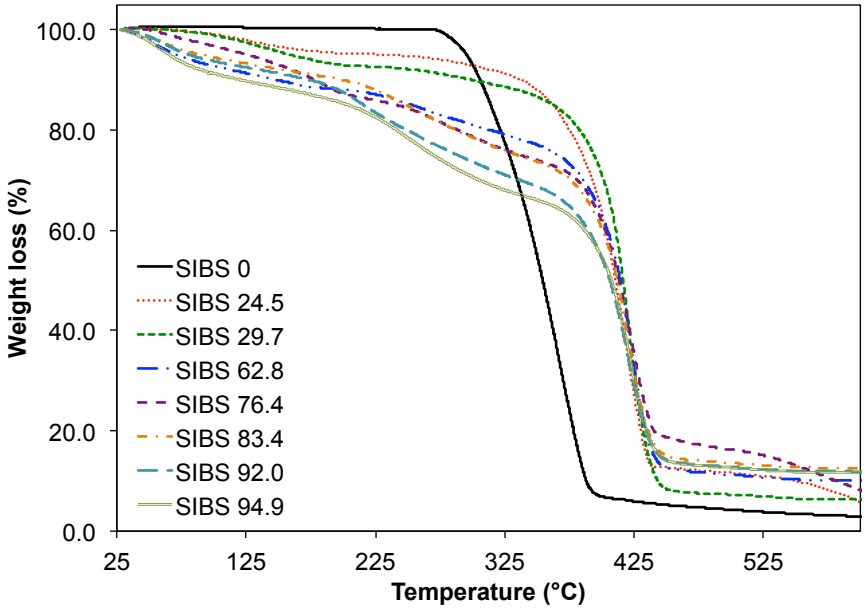

Figure 2.3. TGA curves for SIBS at various sulfonation levels.

Table 2.4. Degradation temperatures for SIBS at various sulfonation levels.

Sample	Degradation temperatures (°C)	
	Sulfonic Group	Backbone
SIBS 0	-	365.39
SIBS 24.5	-	418.08
SIBS 29.7	-	422.96
SIBS 62.8	276.31	422.71
SIBS 76.4	277.45	425.4
SIBS 83.4	251.64	421.08
SIBS 88.5	249.21	426.86
SIBS 90.4	235.49	422.67
SIBS 91.1	232.05	424.27
SIBS 92.0	221.63	420.5
SIBS 94.9	247.68	422.71

The degradation temperature of the cation-substituted membranes is slightly different from the membranes in their acidic form (Figure 2.4 and Table 2.5). The weight loss from 200-370℃ is absent, but in all curves new degradation regions are observed from 430-600℃. These new stages can be attributed to the decomposition of the sulfonic groups that are ionically associated to the counter-ions. The membranes cross-linked with Cu^{+2} show two new stages from 300-385℃ that can also be associated to the sulfonic groups; however, the incorporation of this counter-ion makes the thermal stability of the ionic domains lower than the other counter-ions studied, perhaps because this atom has the highest electronegativity of all counter-ions studied. Detailed results for the degradation temperatures of the sulfonated and counter-ion substituted membranes are summarized in Tables 2.4-2.5 and Appendix C.

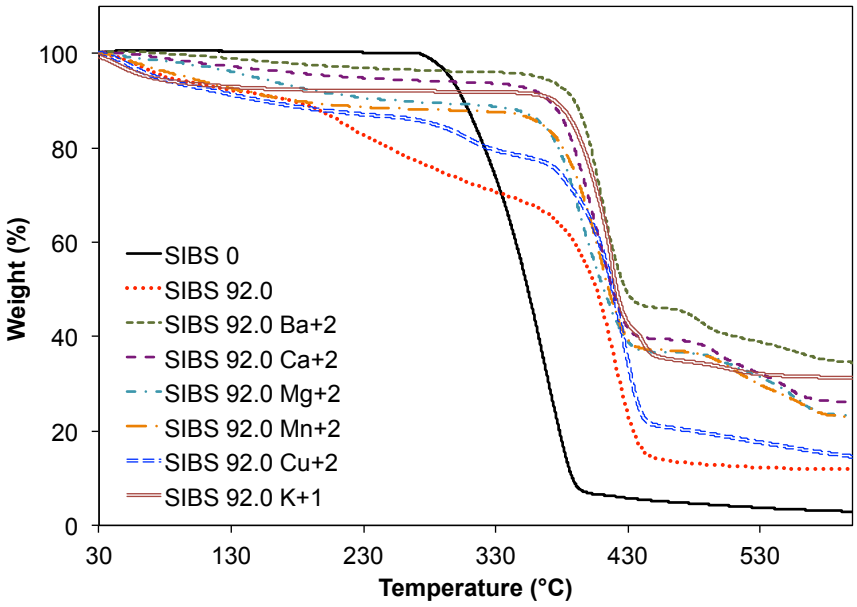

Figure 2.4. TGA curves for counter-ion substituted membranes SIBS 92.0.

Table 2.5. Degradation temperatures for SIBS crosslinked membranes.

Sample	Degradation temperatures (°C)		
	Sulfonic Group	**Backbone**	**Cations**
SIBS 24.5	-	418.08	-
SIBS 24.5 Ba^{+2}	331	411.06	543.29
SIBS 24.5 Ca^{+2}	-	431.95	568.28
SIBS 24.5 Mg^{+2}	-	411.04	556.77
SIBS 24.5 K^{+1}	-	416.91	520.37
SIBS 24.5 Mn^{+2}	-	422.14	532.43
SIBS 24.5 Cu^{+2}	301.75	424.55	-
SIBS 62.8	276.31	422.71	-
SIBS 62.8 Ba^{+2}	-	412.21	467.01/537.71
SIBS 62.8 Ca^{+2}	-	420.28	495.20/552.07
SIBS 62.8 Mg^{+2}	-	413.96	473.40/569.8
SIBS 62.8 K^{+1}	-	414.99	437.20/512.48
SIBS 62.8 Mn^{+2}	-	413.31	474.80/554/49
SIBS 62.8 Cu^{+2}	307.74/385.13	424.87	-
SIBS 92.0	221.63	420.5	-
SIBS 92.0 Ba^{+2}	-	410.66	485.43/560.30
SIBS 92.0 Ca^{+2}	-	403.62	508.31/559.44
SIBS 92.0 Mg^{+2}	-	392.99	505.77/565.09
SIBS 92.0 K^{+1}	-	418.26	456.58/502.21
SIBS 92.0 Mn^{+2}	-	407.78	503.08/561.08
SIBS 92.0 Cu^{+2}	308.68/382.53	427.9	-

2.4.5. TGA-FTIR

Figure 2.5a shows the TGA curve and its corresponding derivative curve for SIBS 92.0 substituted with Ba^{+2}, while Figure 2.5b shows the FTIR spectrums of the outlet gas of the TGA for this run as a function of temperature. From here we can confirm that the weight loss region around 370-430℃ corresponds to the degradation of the polymer backbone chain. It is important to notice that for the Ba^{+2} - substituted membranes - 40% of the sample original weight remains thermally stable at 800℃; this is not the case for other membranes. FTIR spectrum for the sample after the TGA-FTIR experiment was obtained and compared with a previous spectrum obtained before the experiment (Figure 2.5c). It is clear that some of the sulfonic group bands (1124, 1034 cm^{-1}) are missing and

others have lowered their intensity suggesting that the cations may be interacting in different ways with the sulfonic groups.

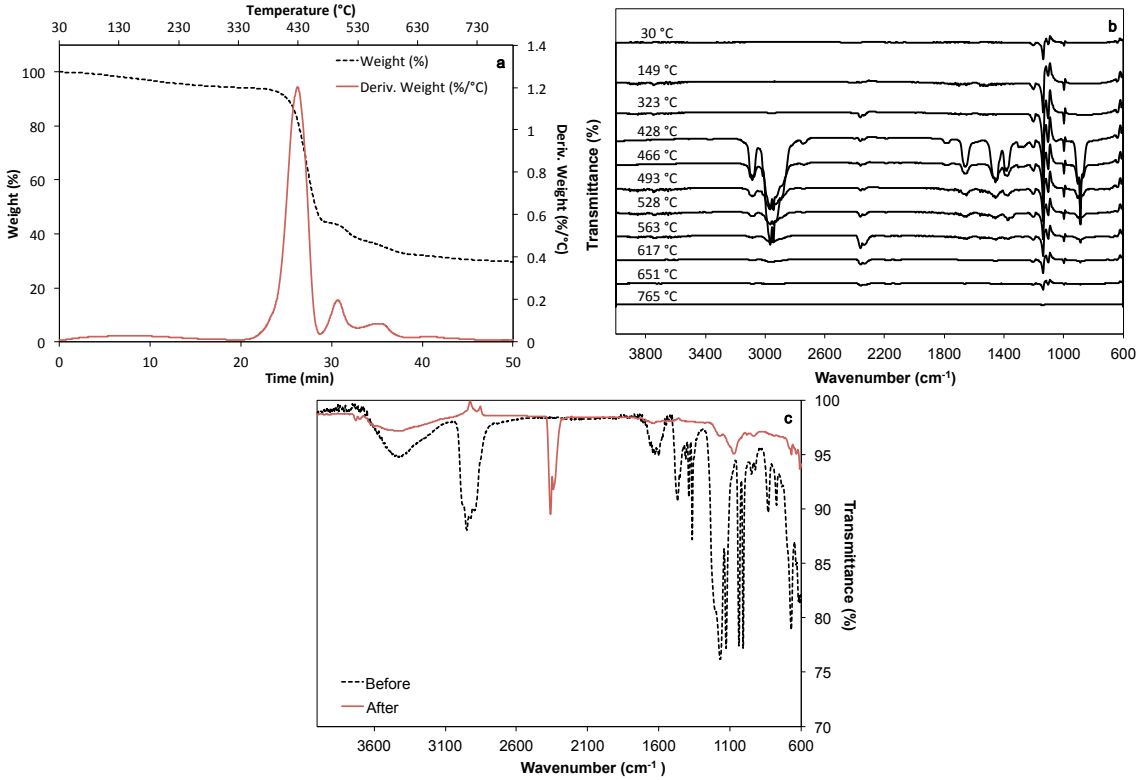

Figure 2.5. TGA-FTIR results for SIBS 92.0 cross-linked with Ba^{+2}: a) Thermogravimetrical analysis results b) Infrared spectra as function of temperature, and c) Infrared spectra before (dash line) and after (solid line) the thermogravimetrical analysis.

2.4.6. Water Swelling

Figures 2.6-2.7 show the water absorption limits for sulfonated and counter-ion substituted SIBS membranes. All membranes reached their equilibrium water swelling in about three hours; however, they were left longer (24 h) to guarantee equilibrium. Figure 6 also shows that the amount of water swelling increases with sulfonation level but up to a maximum, similar to the IEC results. The largest amount of water swelling (up to 558.5 wt. %) was obtained with SIBS 88.5, the highest IEC (not sulfonation level). Above that sulfonation level water swelling decreases perhaps because above that level there are additional interconnected bridges in the three-dimensional structure that inhibit the

accessibility to the ionic domains. The incorporation of counter-ions shows significant differences between the sulfonated and cross-linked membranes (Figure 2.7 and Table 2.6). As Figure 2.7 shows, cation substitution reduces the absorption of water and produces unique swelling for each one of the cations studied.

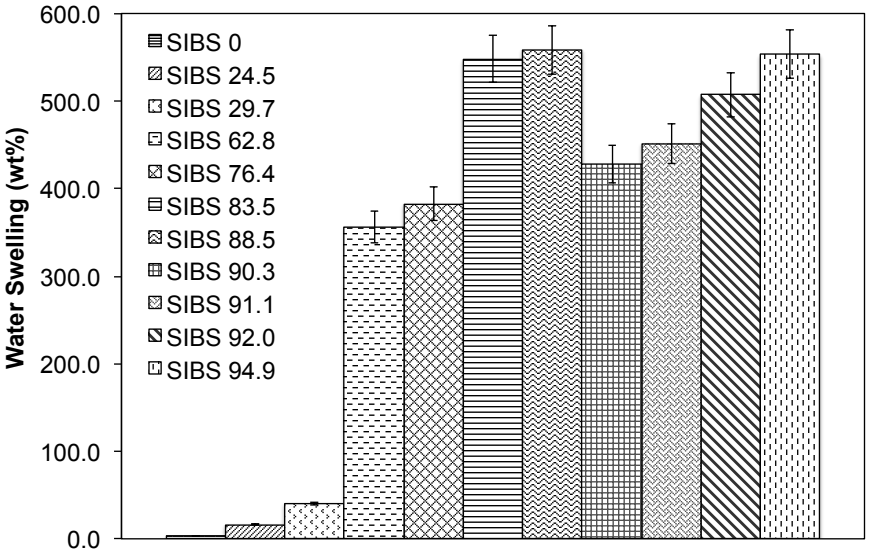

Figure 2.6. Water swelling experiments for SIBS at various sulfonation levels.

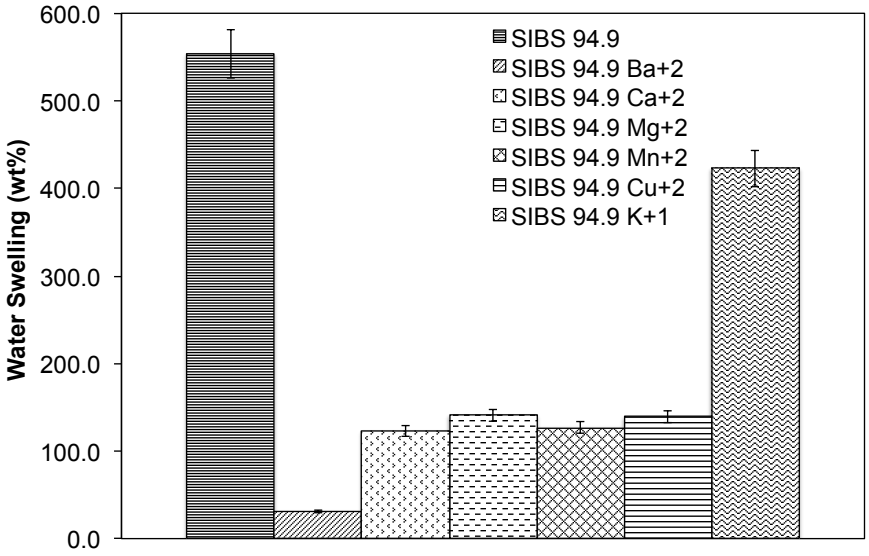

Figure 2.7. Water swelling experiments for counter-ion substituted membranes SIBS 94.9.

Table 2.6. Water absorption limits (wt.%) for SIBS crosslinked membranes.

Sample	Sulfonated	Ba^{+2}	Ca^{+2}	Mg^{+2}	Mn^{+2}	$Cu+^{2}$	K^{+1}
SIBS 29.7	40.43	20.14	19.10	24.19	15.00	18.86	14.72
SIBS 62.8	355.83	26.43	73.41	75.60	82.87	77.67	284.66
SIBS 94.9	553.19	31.10	122.73	141.13	126.72	139.47	422.67

2.4.7. Small Angle X-Ray Scattering

Intensity profiles (I versus q) were obtained normal to the plane for the sulfonated and counter-ion substituted membranes through SAXS experiments. The values of scattering vectors and interstitial (Bragg) distances for the ionic domains are shown in Table 2.7.

Table 2.7. Scattering vector and Bragg distance values for the sulfonated and crosslinked membranes.

Sample	q* (1/nm)	d_{Bragg} (nm)
SIBS 0	0.423	14.85
SIBS 29.7	0.362	17.36
SIBS 29.7 Ba^{+2}	0.362	17.36
SIBS 29.7 Ca^{+2}	0.362	17.36
SIBS 29.7 Mg^{+2}	0.362	17.36
SIBS 29.7 K^{+1}	0.362	17.36
SIBS 62.8	0.342	18.37
SIBS 94.9	0.285	22.05

The scattering vector, q, can be related to the interstitial distance between atoms using Bragg's Law [22,23]

$$d_{Bragg} = \frac{2\pi}{q_{Bragg}} \qquad (2.4)$$

where d_{Bragg} is the distance between aligned atoms and q_{Bragg} is the scattering vector. Due to the weak scattering no periodic pattern was obtained, but the slopes of the curves suggested the presence of different morphologies (Figure 2.8). It is important to mention

that as sulfonation increases, the Bragg distance between crystalline domains increases (Table 2.7). Counter-ion substituted SIBS 29.7 shows an increase in the intensity of the curve, but no significance difference in the interstitial distance for different cations, especially around the ionomer peak (Figure 2.9, Table 2.7). This suggests that the cations do not affect the size of the ionic nanochannels, but as it has been presented and will be presented ahead, they influence the equilibrium and transport properties through the membrane.

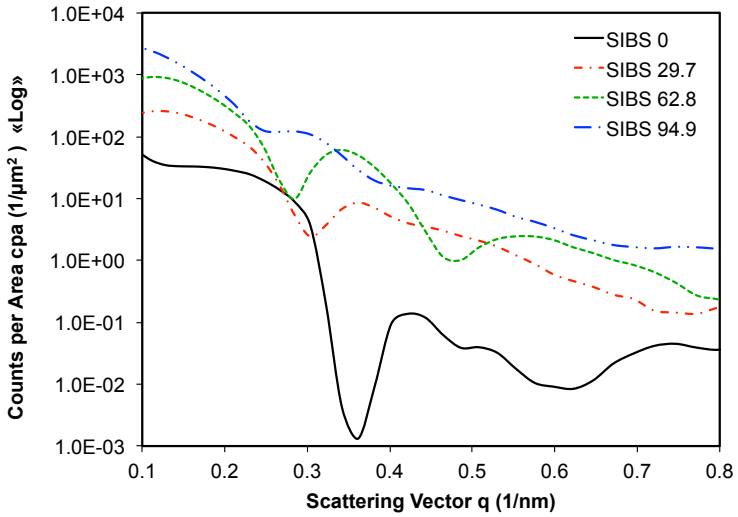

Figure 2.8. Small-angle X-ray scattering profiles for SIBS at various sulfonation levels.

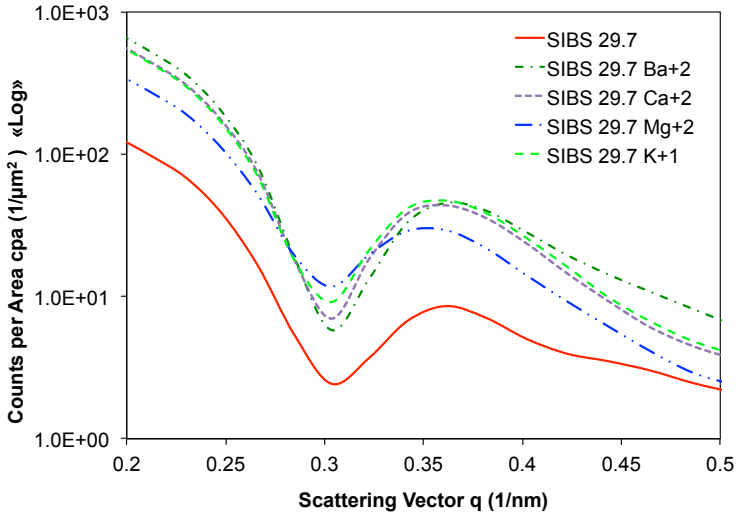

Figure 2.9. Small-angle X-ray scattering profiles for cross-linked SIBS 29.7 membranes.